Plasma heating and particle acceleration in collisionless shocks through astrophysical observations

M Miceli

Dipartimento di Fisica e Chimica E. Segrè, Università degli Studi di Palermo, Piazza del Parlamento 1, 90134 Palermo, Italy

INAF-Osservatorio Astronomico di Palermo, Piazza del Parlamento 1, 90134 Palermo, Italy

E-mail: marco.miceli@unipa.it

Abstract

Supernova remnants (SNRs), the products of stellar explosions, are powerful astrophysical laboratories, which allow us to study the physics of collisionless shocks, thanks to their bright electromagnetic emission. Blast wave shocks generated by supernovae (SNe) provide us with an observational window to study extreme conditions, characterized by high Mach (and Alfvénic Mach) numbers, together with powerful nonthermal processes. In collisionless shocks, temperature equilibration between different species may not be reached at the shock front. In this framework, different particle species may be heated at different temperatures (depending on their mass) in the post-shock medium of SNRs. SNRs are also characterized by broadband nonthermal emission stemming from the shock front as a result of nonthermal populations of leptons and hadrons. These particles, known as cosmic rays, are accelerated up to ultrarelativistic energies via diffusive shock acceleration. If SNRs lose a significant fraction of their ram energy to accelerate cosmic rays, the shock dynamics should be altered with respect to the adiabatic case. This shock modification should result in an increase in the total shock compression ratio with respect to the Rankine–Hugoniot value of 4. Here, I show that the combination of x-ray high resolution spectroscopy (to measure ion temperatures) and moderate resolution spectroscopy (for a detailed diagnostic of the post-shock density) can be exploited to study both the heating mechanism and the particle acceleration in collisionless shocks. I report on new results on the temperatures measured for different ion species in the remnant of the SN observed in 1987 in the Large Magellanic Cloud (SN 1987A). I also discuss evidence of shock modification recently obtained in the remnant of SN 1006 a. D., where the shock compression ratio increases significantly as the angle between the shock velocity and the ambient magnetic field is reduced.

Keywords: plasmas, shock waves, acceleration of particles

(Some figures may appear in colour only in the online journal)

1. Introduction

Astrophysical shocks are ubiquitous in the Universe, showing a wide variety of Mach numbers and characteristic length-scales. Astrophysical shocks are typically collisionless, because they expand in a rarefied medium, where Coulomb collisions cannot provide viscous dissipation at the shock front. Collisionless shocks have indeed been observed at all
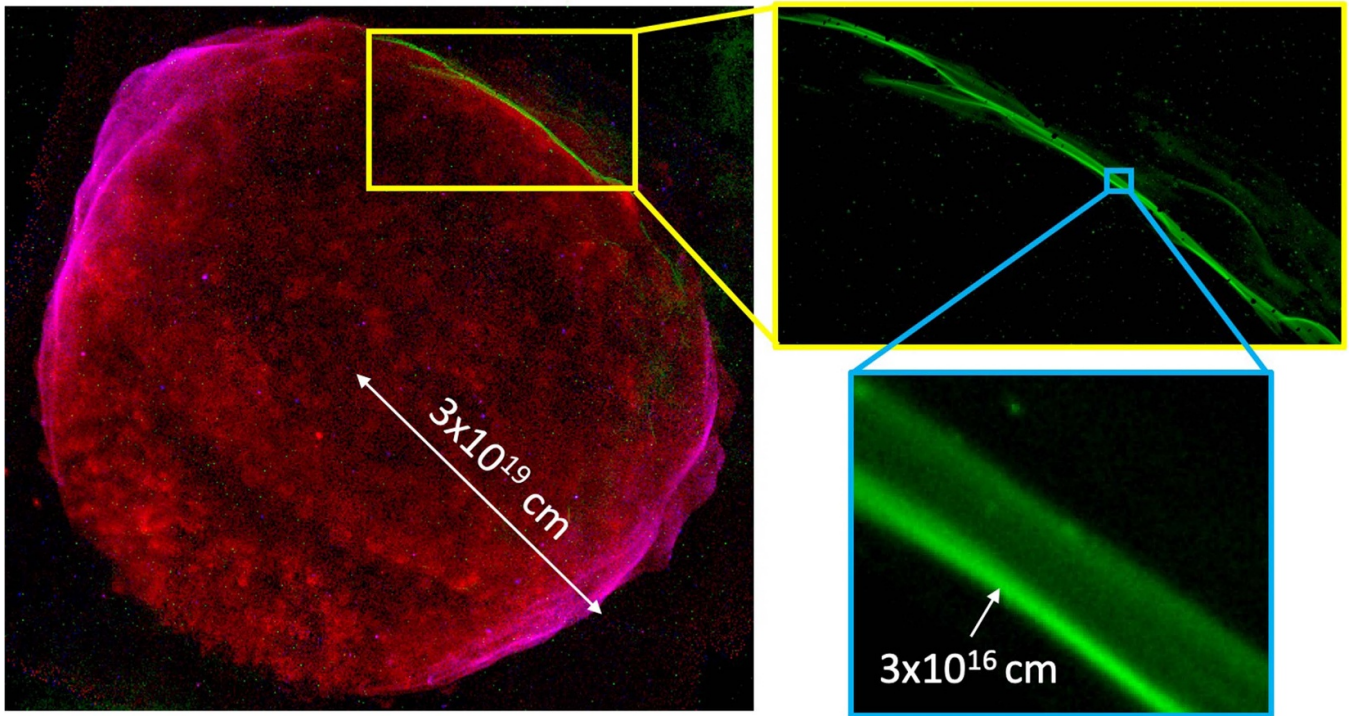
Figure 1. *Left-hand panel*: Flux images of SN 1006 in the 0.5–1 keV (red) and 2.5–7 keV (blue) bands, obtained with the *Chandra x-ray telescope*, together with Balmer Hα emission (green). *Right panels:* close-up views of the Hα filament marking the shock front. In all panels North is up and East is to the left. Physical scales (indicated by white arrows) were obtained for a distance of 2.2 kpc [20].

scales, ranging from small, 'local' shocks in the solar wind [1] up to giant, cosmological shock waves [2].

Supernova remnants (SNRs) are the leftovers of supernova (SN) explosions and are characterized by powerful collisionless shocks. Their birth is associated with a sudden (less than one second) release of a large amount of energy, which is of the order of $E = 10^{53}$ erg for core-collapse supernovae (SNe) and $E = 10^{51}$ erg for Type Ia SNe (associated with the explosion of a white dwarf). Both core-collapse and Type Ia SN explosions determine the violent ejection of supersonic stellar fragments (ejecta), having a characteristic kinetic energy of 10^{51} erg (which corresponds to the energy that the Sun would radiate if it were to maintain its current luminosity for almost 16 billion years, i.e. more than the age of the Universe). The velocity profiles of the ejecta can reach values as high as a few 10^4 km s^{-1} and their expansion and deceleration in the interstellar medium (ISM) drive strong shocks, which compress and heat the ambient medium (forward shocks) and the ejecta themselves (reverse shocks) up to x-ray emitting temperatures.

X-ray observations of SNRs show spectacular extended nebulae, which reveal the complex morphology of shocked ISM and ejecta, and convey a wealth of information on many aspects of the remnant origin and evolution, and on the shock physics. Figure 1 shows a composite image of the remnant of the SN exploded in 1006 A. D. (hereafter SN 1006). Soft x-rays (0.5–1 keV, in red) show a complex pattern, with ripples of emission revealing knots of shocked ejecta [3, 4], hard x-rays (2.5–7 keV, in blue) are associated with

synchrotron radiation in the northeastern and southwestern limbs [5], while optical H$_\alpha$ emission (in green) marks the northwestern shock front in great detail. By considering characteristic values for the post-shock temperature and density ($T = 10^7$ K [3], and $n = 0.1$ cm^{-3} [6, 7], respectively), the Coulomb collision mean free path is of the order of 10^{19} cm, i.e. comparable with the radius of the remnant and much larger than the width of the shock front. Since the viscous dissipation at the shock front is localized in an extremely narrow region, it cannot be provided by collisions and collective effects, such as electromagnetic fluctuations and plasma waves, are instead thought to be responsible for the plasma heating. Indeed in this case, the shock width might be of the order of 10^8 cm, given that the ion inertial length for SN 1006 is of approximately 10^8 cm, and the proton gyroradius for protons with the same speed as the shock (5000 km s^{-1} [4]) in a magnetic field of 90 μG [8, 9] is of approximately 5×10^8 cm.

The sudden heating and compression within the thin shock front is followed by a slow relaxation toward equilibrium in the downstream flow. Therein, the almost neutral optically thin coronal plasma is slowly ionized through electron–ion collisions, and reaches collisional ionization equilibrium only after a timescale of approximately $t_{CIE} = 10^{12}/n$ s (where n is the post shock density in cm^{-3}, [10]), which corresponds to more than 10^5 yr for the typical densities of SN 1006, i.e. more than ten times the age of the remnant. It is then unsurprising that the x-ray spectra of SNRs typically show signatures of an under ionized plasma, though with some notable exception (e.g. W49B [11–13], IC 443 [14–16] and W44 [17]).

Moreover, different particle species are expected to be heated at different temperatures in collisionless shocks, and their thermalization proceeds slowly in the post shock medium. For example, the time-scale for electron–proton temperature equilibration is $t_{ep} \sim 10^4 n^{-1}(kT/1\,\mathrm{keV})^{3/2}(\ln\Lambda/31)$ yr, which can be as well larger (much larger for historical SNRs) than the age of a remnant. For example, in SN 1006, $t_{ep} \sim 10^5$ yr. In general, therefore, the shocked plasma in SNRs is *not* in equilibrium.

Shock fronts in SNRs are known to be powerful particle accelerators, with particles gaining energy by diffusively crossing the shock front back and forth through the first-order Fermi mechanism (or diffusive shock acceleration). Radio synchrotron radiation from ultrarelativistic (GeV) electrons is systematically observed in the shell of SNRs [18], and x-ray synchrotron emission from electrons, with energies reaching $\sim 10^{13}$ eV can be observed at the shock fronts of young SNRs [19], including SN 1006 (see figure 1). Evidence for high energy hadrons in SNRs has also been obtained in a few cases [21–24].

Here, I first focus on the shock heating mechanism and on the evolution of the ion temperature in the shocked plasma in the remnant of the SN observed on 1987 February 23 in the Large Magellanic Cloud (hereafter SN 1987A). I will then show the effects of the back-reaction of hadron acceleration on the shock front of SN 1006.

The paper is organized as follows: section 2 is dedicated to the collisionless shock heating in SN 1987A, section 3 shows the shock modification induced by efficient particle acceleration in SN 1006, while my conclusions are summarized in section 4

2. Collisionless shock heating in SN 1987A

In a collisionless shock propagating in a medium with different particle species, by adopting a multi-fluid approach, one may be tempted to write down the Rankine–Hugoniot conditions for each particle species. In this framework, the post-shock temperature T_i for the ith species might be obtained from the relation:

$$kT_i = \frac{3}{16}m_i v_{sh}^2 \qquad (1)$$

where m_i is the particle mass for the ith species and v_{sh} is the shock velocity. A mass-proportional post-shock temperature is expected in the case of scattering isotropization of the incoming particles by plasma waves. However, this approach does not consider that (partial) equilibration between different species can also occur within the shock front (e.g. by wave-particle interactions).

It is not straightforward to test the validity of equation (1) by considering protons and electrons. This is because the processes responsible for electron heating in collisionless shocks are expected to be different from those acting for protons and ions [2, 25, 26]. Indeed, the electron-to-proton temperature

ratio in SNRs is lower than 1, though being typically larger than that predicted by equation (1) [27–30], and showing a dependence on the shock velocity, which can be described by $T_e/T_p \propto v_{sh}^{-2}$ [31].

To test whether in collisionless shocks the post-shock temperature scales linearly with the particle mass, it is then crucial to measure the temperature of ions with different masses in the shocked plasma. Early UV observations of SN 1006 indicated an oxygen to proton temperature ratio larger than 1, but lower than that predicted by equation (1) [32]. However, more recent measurements have shown mass-proportional heating for He, C and N ions in the same remnant. Since bright emission line complexes of heavy ions are typically observed in the x-ray band, the analysis of x-ray spectra is crucial to extend the study of collisionless particle heating to a wider range of masses.

The temperature of ions can be deduced from the thermal broadening of their x-ray emission lines [33, 34]. This is a delicate measurement since different effects contribute to the line broadening of an emission line stemming in the plasma of an SNR, namely (a) the intrinsic resolution of the x-ray spectrometers, (b) the bulk Doppler motion (if approaching and receding plasmas lie along the same line of sight); (c) the angular extension of the x-ray emission (current high resolution spectrometers are typically slitless, so the spectrum is convolved with the profile of the remnant emission in the dispersion direction), and (d) thermal broadening. It is then crucial to disentangle the contribution of thermal broadening from other effects to get an accurate measurement of the ion temperatures.

To this end, SN 1987A is a privileged target: its x-ray emission has been monitored regularly, thus providing a unique dataset for the evolution of the x-ray spectra in a young SNR. Moreover, x-ray data are complemented by a wealth of observations in an extremely wide range of wavelengths (from radio to $\gamma-$rays), which provided us with accurate diagnostics of the complex interaction of the shock front with the surrounding inhomogeneous medium [35, 36]. The constraints derived from the multi-epoch and multi-wavelength observations were adopted as setup parameters to develop a thorough 3D magnetohydrodynamic (MHD) model, which is able to describe in great detail both the origin and the evolution of the remnant and of its thermal and nonthermal emission self-consistently. In particular, the model setup includes a thorough representation of the circumstellar medium, characterized by an extended H II region and a dense, knotty, equatorial ring, in agreement with observations. The 3D model describes both the SN explosion and the interaction of the remnant with the inhomogeneous circumstellar environment, by carefully reproducing the bolometric SN light curve, the subsequent x-ray and radio light curves (from the explosion to the present day), together with the evolution of the radio and x-ray morphology of the remnant in the last 35 years. Remarkably, the MHD model is also able to reproduce the multi-epoch x-ray spectra of SN 1987A [37–40]. A novel approach combining data and the MHD model was developed to analyze the high resolution x-ray spectra of SN 1987A collected with the *Chandra* x-ray telescope [41]. This work focused on 2007 and 2011 data,

i.e. the two deepest observations performed with the *Chandra* High Energy Transmission Grating (HETG) available at that time. The method relies on the measurement of the line broadening of Ne, Mg, Si and Fe emission lines from the actual x-ray spectra. The contribution to the line broadening associated with the bulk velocity of the expanding emitting plasma (Doppler broadening) is then derived from the MHD model. For all the lines inspected, the combination of bulk Doppler broadening and instrumental broadening significantly underestimates the observed line widths. It is then possible to ascertain the additional contribution of thermal broadening which is needed to reproduce the observed widths of the ion lines, thus measuring the corresponding ion temperatures. An accurate comparison of the actual spectra with those synthesized from the MHD model, made it possible to derive the post-shock temperatures of Ne, Mg, Si and Fe. The results clearly show that, for these species, the ion to proton temperature ratio is always significantly higher than one and is consistent with increasing linearly with the ion mass, as predicted by equation (1), for a wide range shock parameter [41]. A similar methodology was later adopted to analyze the Chandra HETG observations taken in 2018 [42], confirming that, on average, the observed line widths are well described when thermal broadening associated with mass proportional heating is taken into account.

I here combine the results obtained for 2007–2011 [41] spectra with those obtained for the 2018 observation [42]. By adopting the procedure described in [41], I compare the actual line widths with those predicted by the MHD model with and without including the effects of thermal broadening, thus determining the ion temperature. Figure 2 shows the ion to proton temperature ratio for Ne, Mg, Si and Fe, together with the mass-proportional relation predicted by equation (1). The general trend clearly confirms previous results and is in remarkable agreement with predictions of hybrid simulations of collisionless shocks, which show that the post shock temperature scales linearly with the atomic mass A (with simulations performed up to $A = 8$, [43]).

On the other hand, figure 2 shows that the post-shock temperature of Mg is slightly lower than expected. The measured Mg temperature mainly depends on the width of its brightest emission line, namely the Lyα for the ionization state Mg XII at ∼8.4 Å. A possible explanation for the relatively low temperature of Mg is that this emission line stems well behind the shock front, in a region where ions are approaching thermal equilibrium with other particles, and the temperature is expected to be lower than that achieved at the shock front. Temperature equilibration between ions and protons is expected to be reached when the time integral of the electron density reaches $\tau \sim 5 - 10 \times 10^{10}$ s cm^{-3} [44]. On the other hand, it must be considered that the thermalization timescale increases by about a factor of 5 [45] in a very turbulent magnetic field, which is expected to be present in the SN 1987A shocked medium [46]. This suggests that significant temperature variations with respect to the immediate post-shock region are expected for those ions whose emission lines originate in a
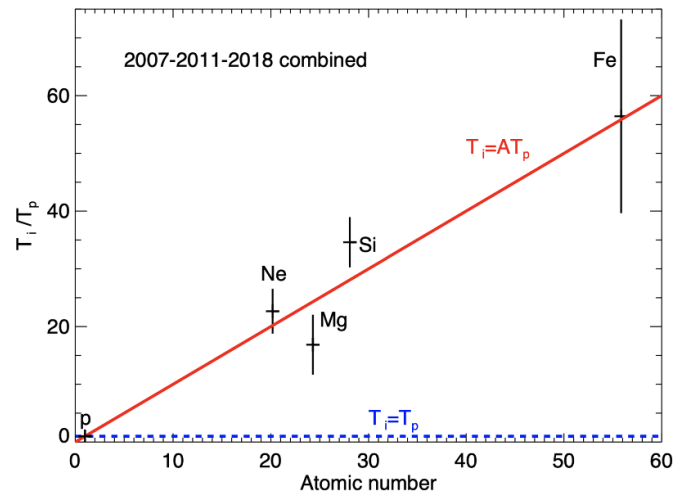

Figure 2. Ion to proton temperature ratios for Ne, Mg, Si and Fe in SN 1987A were obtained by combining the 2007 and 2011 results [41] with the 2018 results [42]. The red line marks the mass-proportional trend predicted by equation (1).

plasma with τ larger than $\sim 2 - 5 \times 10^{11}$ s cm^{-3}. The MHD model adopted to synthesize the spectra includes Coulomb collisions between electrons and protons and follows their temporal evolution downstream, while collisions between ions and protons are not included. However, from the synthetic spectra, it is possible to derive the contribution to the line emission stemming from a given value of τ and temperature of the plasma. I here focus on the synthetic spectra extracted from model B18.3 ([40], see also [47] for a similar approach to the Fe K line emission) describing SN 1987A 31 years after the explosion (corresponding to 2018 a. D.).

Figure 3 shows the characteristic values of temperature and ionization parameter of the plasma, which mainly contributes to the line emission. In particular, left panel of figure 3 shows the normalized continuum-subtracted line flux of the Mg XII emission line as a function of the plasma temperature (vertical axis, kT) and ionization parameter (horizontal axis, τ). This figure clearly shows that the bulk of the emission line originates in a region where the ionization parameter τ is slightly larger than 10^{11} s cm^{-3}, i.e. where thermalization between Mg and colder protons starts to be relevant (the value $\tau = 10^{11}$ s cm^{-3} is marked by the vertical dashed line in figure 3). This is in good agreement with the Mg showing a lower temperature than that expected at the shock front. As a comparison, I also report the distribution of the continuum-subtracted line flux as a function of kT and τ for the Si XIII emission line (Heα at 6.65 Å, right panel of figure 3), which is the brightest Si line (i.e. the estimate of the Si temperature mainly depends on its width): in this case the bulk of the line emission originates from a plasma with $\tau < 10^{11}$ s cm^{-3}, where we expect the ion temperature to be almost the same as that achieved at the shock front.

Further investigations require the inclusion of ion–proton collisions in the model. However, this approach already
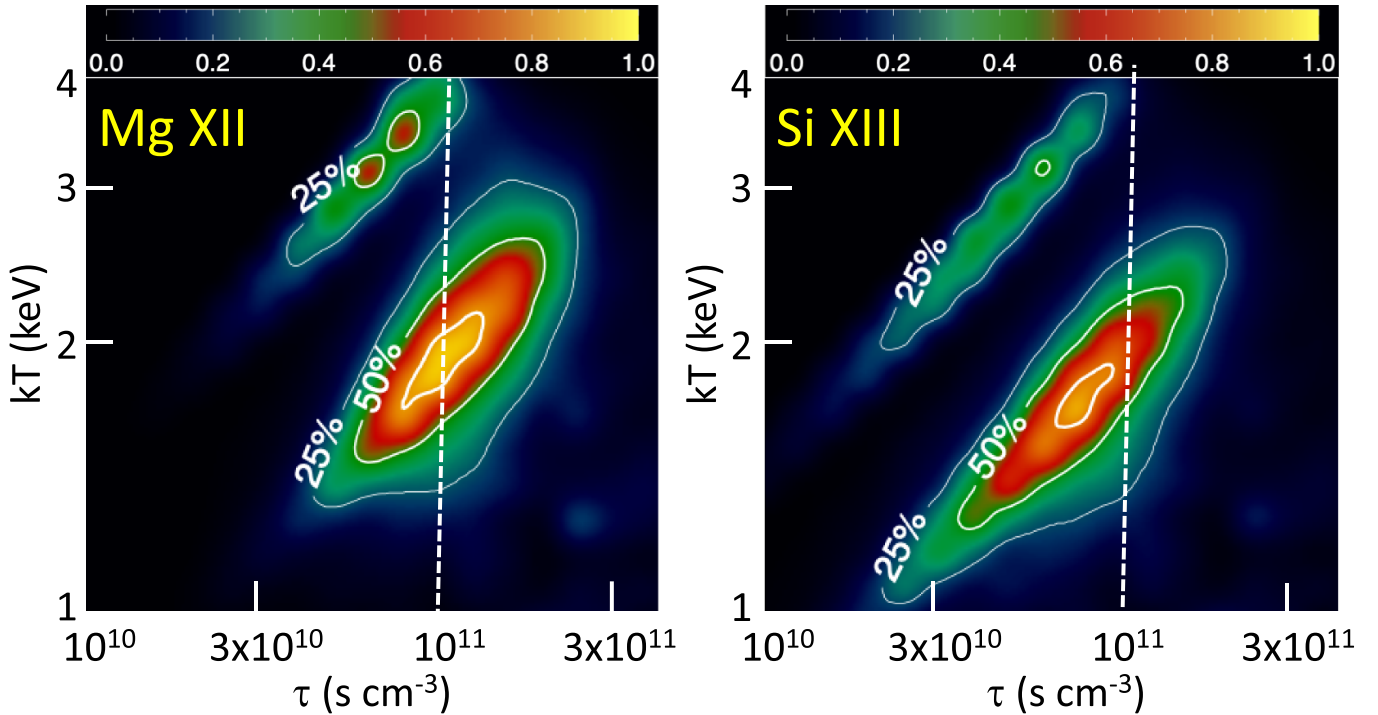
Figure 3. Normalized continuum-subtracted line flux of the Mg XII Lyα (*left panel*) emission line and of the Si XIII Heα (*right panel*) emission line as a function of the plasma temperature and time integral of the electron density (τ). Contours mark 25%, 50% and 75% of the maximum.

shows that the combination of data analysis and MHD modeling provides a powerful diagnostic tool to study both the immediate post-shock conditions and the evolution toward equilibrium in the post-shock flow.

3. Shock modification in SN 1006

As explained in section 1, collisionless shock heating is associated with particle acceleration and SNRs are known to be sites of efficient acceleration. Self-consistent hybrid (kinetic ion-fluid electrons) simulations show that the acceleration efficiency is expected to increase by reducing the angle between the shock velocity and the ambient magnetic field and that magnetic turbulences are associated with efficient ion acceleration (quasi-parallel scenario, e.g. [48]). This is in agreement with measurements of radio polarization. For example, the radio polarization study of SN 1006 shows efficient particle acceleration and higher magnetic turbulence for quasi-parallel shocks [49]. Similarly, radio polarization measurements in Kepler's SNR indicate an almost radial (i.e. parallel to the shock velocity) magnetic field and a lower level of polarization [50], which is indicative of high magnetic turbulence at the acceleration site [51]. On the other hand, the re-acceleration of ambient cosmic-ray seeds is nearly independent of the shock inclination [52].

Indeed, SNRs can sustain the observed flux of Galactic cosmic rays, provided that they inject 10%–20% of their kinetic energy into the particles (e.g. [53]). Such an effect, if present, is expected to alter the shock dynamics by increasing the shock compression ratio and decreasing the post-shock temperature with respect to the Rankine–Hugoniot values [24, 54–57]. In particular, recent hybrid simulations show the formation of a shock postcursor associated with efficient particle acceleration. The postcursor moves downstream (approximately at the Afvén speed), acting as an additional energy sink, which allows non-linear magnetic fluctuations and particles, to drift away from the shock front [58]. When the effects of the postcursor are taken into account, a shock compression ratio $r_s \sim 6$–7 (to be compared with the canonical value of 4 for strong shocks) can be achieved when the cosmic ray pressure is of the order of 10% of the bulk ram pressure.

The presence of shock modification has been recently revealed in SN 1006 [7]. Thanks to the almost uniform magnetic field in this remnant, approximately aligned in the southwest-northeast direction, it is possible to observe, in the same object, regions with efficient particle acceleration (i.e. regions in quasi-parallel conditions, as indicated by the blue limbs in figure 1) and regions where we do not expect shock modification [6]. A careful spatially resolved spectral analysis of the x-ray spectra stemming from the shocked ISM at different positions of the shell reveals a regular azimuthal modulation of r_s, with a minimum $r_s = 4$ in quasi-perpendicular conditions and a maximum, which reaches values as high as $r_s = 7$ in quasi-parallel conditions [7]. Figure 4 shows the azimuthal profile of the shock compression ratio (as a function of the angle between the shock velocity and the ambient magnetic field) derived for SN 1006. The accurate comparison of the azimuthal profile of the shock compression ratio with state of the art theoretical models of modified shocks
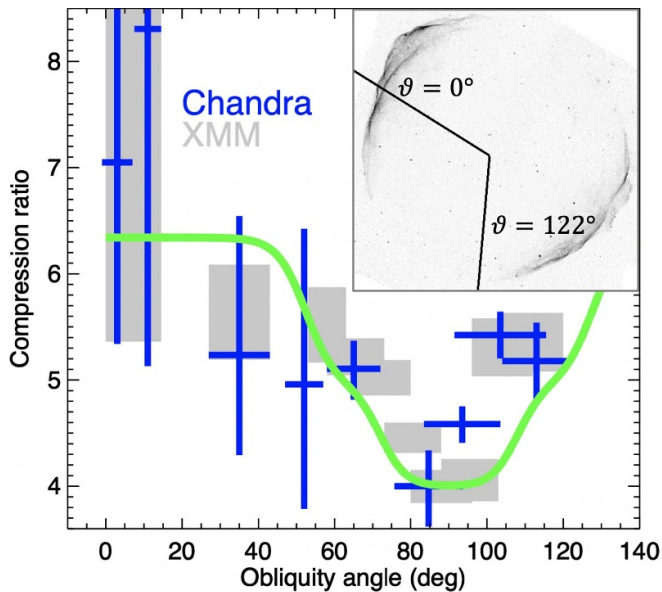
Figure 4. The azimuthal profile of the shock compression ratio in SN 1006 is derived from the analysis of *Chandra* (blue crosses) and *XMM-Newton* (gray boxes) spectra by [7]. Error bars are at the 68% confidence level. The inset in the upper right corner shows the *Chandra* x-ray map of SN 1006 in the 2–4.5 keV band to highlight the sector of the remnant analyzed. The green curve shows the expected profile proposed by [7] for normalized pressure of cosmic rays $\xi_p = 12\%$, normalized magnetic pressure $\xi_B = 5\%$, and cosmic ray re-acceleration efficiency $\xi_s = 6\%$. The configuration of the ambient magnetic field is as in [59].

including the effect of the postcursor (indicated by the green curve in figure 4) shows a nice agreement between model and observations and provides important constraints on the acceleration efficiency and on its dependence on the angle between the ambient magnetic field and the shock velocity. In particular, in quasi-parallel conditions, the cosmic ray pressure is ∼12% of the total, while the normalized magnetic pressure is ∼5%. Moreover, the r_s azimuthal profile shows a sharp minimum, which is strongly indicative of efficient (normalized pressure ∼6%) re-acceleration of pre-existing Galactic cosmic rays [7].

The shock modification is expected to affect the spectrum of the accelerated particles, by modifying their spectral index [60]. Remarkably, when considering the model parameters that best reproduce the azimuthal profile of r_s, a spectral index of ∼2.2 is obtained for the energy spectrum in the regions with maximum acceleration efficiency (the nonthermal limb). When considering the synchrotron emission from the accelerated electrons, this corresponds to a photon index $\alpha \sim 0.6$, which is in nice agreement with that observed for SN 1006 [18].

4. Conclusion

Astrophysical shocks are natural laboratories, which allow us access to the shock physics at extreme conditions. X-ray observations of SNRs are a powerful diagnostic tool to study the abrupt collisionless shock heating and the relaxation

of the post-shock plasma toward equilibrium. Also, x-ray observations allow us to observe synchrotron radiation from ultrarelativistic electrons accelerated at the shock front and to probe the back-reaction of cosmic rays on the shock dynamics [61].

To extract all the information stored in the x-ray data, a detailed comparison with state-of-the-art models is necessary.

The physical processes localized at the shock front affect the whole remnant structure and its global evolution. Therefore, both hybrid simulations investigating the microphysics at the shock front and MHD models describing the evolution of the system on larger spatial and time scales provide powerful tools to achieve a higher level of diagnostics.

Moreover, the upcoming generation of x-ray telescopes (as *XRISM* and *Athena*) will be equipped with high resolution spectrometers, based on microcalorimeters, which will provide us with an unprecedented level of detail. The development of novel advanced tools for data analysis and for quantitative comparison with theoretical models is a challenging task, which will allow us to exploit the quality of the data in the near future.

Data availability statement

The data that support the findings of this study are available upon reasonable request from the authors.

Acknowledgment

ORCID iD

M Miceli ⬥ https://orcid.org/0000-0003-0876-8391

References

[1] Tsurutani B T and Stone R G 1985 *Collisionless Shocks in the Heliosphere: Reviews of Current Research* (*Geophysical Monograph Series* vol 35) (Washington, DC: American Geophysical Union)

[2] Bykov A M, Dolag K and Durret F 2008 *Space Sci. Rev.* **134** 119–40

[3] Miceli M, Bocchino F, Iakubovskyi D, Orlando S, Telezhinsky I, Kirsch M G F, Petruk O, Dubner G and Castelletti G 2009 *Astron. Astrophys.* **501** 239–49

[4] Williams B J, Borkowski K J, Ghavamian P, Hewitt J W, Mao S A, Petre R, Reynolds S P and Blondin J M 2013 *Astrophys. J.* **770** 129

[5] Koyama K, Petre R, Gotthelf E V, Hwang U, Matsura M, Ozaki M and Holt S S 1995 *Nature* **378** 255

[6] Miceli M, Bocchino F, Decourchelle A, Maurin G, Vink J, Orlando S, Reale F and Broersen S 2012 *Astron. Astrophys.* **546** A66

[7] Giuffrida R, Miceli M, Caprioli D, Decourchelle A, Vink J, Orlando S, Bocchino F, Greco E and Peres G 2022 *Nat. Commun.* **13** 5098

[8] Morlino G, Amato E, Blasi P and Caprioli D 2010 *Mon. Not. R. Astron. Soc.* **405** L21–25

[9] Ballet J 2006 *Adv. Space Res.* **37** 1902–8

[10] Smith R K and Hughes J P 2010 *Astrophys. J.* **718** 583–5

[11] Ozawa M, Koyama K, Yamaguchi H, Masai K and Tamagawa T 2009 *Astrophys. J. Lett.* **706** L71–L75

[12] Miceli M, Bocchino F, Decourchelle A, Ballet J and Reale F 2010 *Astron. Astrophys.* **514** L2

[13] Yamaguchi H *et al* 2018 *Astrophys. J. Lett.* **868** L35

[14] Kawasaki M, Ozaki M, Nagase F, Inoue H and Petre R 2005 *Astrophys. J.* **631** 935–46

[15] Greco E, Miceli M, Orlando S, Peres G, Troja E and Bocchino F 2018 *Astron. Astrophys.* **615** A157

[16] Okon H, Tanaka T, Uchida H, Tsuru T G, Seta M, Kokusho T and Smith R K 2021 *Astrophys. J.* **921** 99

[17] Okon H *et al* 2020 *Astrophys. J.* **890** 62

[18] Green D A 2019 *J. Astrophys. Astron.* **40** 36

[19] Vink J 2012 *Astron. Astrophys. Rev.* **20** 49

[20] Winkler P F, Gupta G and Long K S 2003 *Astrophys. J.* **585** 324–35

[21] Tavani M *et al* 2010 *Astrophys. J. Lett.* **710** L151–5

[22] Morlino G and Caprioli D 2012 *Astron. Astrophys.* **538** A81

[23] Ackermann M *et al* 2013 *Science* **339** 807–11

[24] Slane P, Lee S H, Ellison D C, Patnaude D J, Hughes J P, Eriksen K A, Castro D and Nagataki S 2014 *Astrophys. J.* **783** 33

[25] Shimada N and Hoshino M 2000 *Astrophys. J. Lett.* **543** L67–71

[26] Park J, Caprioli D and Spitkovsky A 2015 *Phys. Rev. Lett.* **114** 085003

[27] Rakowski C E, Ghavamian P and Hughes J P 2003 *Astrophys. J.* **590** 846–57

[28] Ghavamian P, Schwartz S J, Mitchell J, Masters A and Laming J M 2013 *Space Sci. Rev.* **178** 633–63

[29] Raymond J C 2018 *Space Sci. Rev.* **214** 28

[30] van Adelsberg M, Heng K, McCray R and Raymond J C 2008 *Astrophys. J.* **689** 1089–104

[31] Ghavamian P, Laming J M and Rakowski C E 2007 *Astrophys. J.* **654** L69–L72

[32] Korreck K E, Raymond J C, Zurbuchen T H and Ghavamian P 2004 *Astrophys. J.* **615** 280–5

[33] Vink J, Laming J M, Gu M F, Rasmussen A and Kaastra J S 2003 *Astrophys. J. Lett.* **587** L31–L34

[34] Broersen S, Vink J, Miceli M, Bocchino F, Maurin G and Decourchelle A 2013 *Astron. Astrophys.* **552** A9

[35] McCray R 1993 *Annu. Rev. Astron. Astrophys.* **31** 175–216

[36] McCray R and Fransson C 2016 *Annu. Rev. Astron. Astrophys.* **54** 19–52

[37] Orlando S, Miceli M, Pumo M L and Bocchino F 2016 *Astrophys. J.* **822** 22

[38] Orlando S *et al* 2019 *Astron. Astrophys.* **622** A73

[39] Ono M, Nagataki S, Ferrand G, Takahashi K, Umeda H, Yoshida T, Orlando S and Miceli M 2020 *Astrophys. J.* **888** 111

[40] Orlando S *et al* 2020 *Astron. Astrophys.* **636** A22

[41] Miceli M, Orlando S, Burrows D N, Frank K A, Argiroffi C, Reale F, Peres G, Petruk O and Bocchino F 2019 *Nature Astronomy* **3** 236–41

[42] Ravi A P, Park S, Zhekov S A, Miceli M, Orlando S, Frank K A and Burrows D N 2021 *Astrophys. J.* **922** 140

[43] Caprioli D, Yi D T and Spitkovsky A 2017 *Phys. Rev. Lett.* **119** 171101

[44] Spitzer L 1962 *Physics of Fully Ionized Gases* 2nd edn (New York: Interscience)

[45] Narayan R and Medvedev M V 2001 *Astrophys. J. Lett.* **562** L129–32

[46] Zanardo G, Staveley-Smith L, Gaensler B M, Indebetouw R, Ng C Y, Matsuura M and Tzioumis A K 2018 *Astrophys. J. Lett.* **861** L9

[47] Greco E *et al* 2022 *Astrophys. J.* **931** 132

[48] Caprioli D and Spitkovsky A 2014 *Astrophys. J.* **783** 91

[49] Reynoso E M, Hughes J P and Moffett D A 2013 *Astron. J.* **145** 104

[50] DeLaney T, Koralesky B, Rudnick L and Dickel J R 2002 *Astrophys. J.* **580** 914–27

[51] Sapienza V, Miceli M, Bamba A, Katsuda S, Nagayoshi T, Terada Y, Bocchino F, Orlando S and Peres G 2022 *Astrophys. J.* **935** 152

[52] Caprioli D, Zhang H and Spitkovsky A 2018 *J. Plasma Phys.* **84** 715840301

[53] Hillas A M 2005 *J. Phys. G: Nucl. Phys.* **31** R95–R131

[54] Drury L O 1983 *Rep. Prog. Phys.* **46** 973–1027

[55] Decourchelle A, Ellison D C and Ballet J 2000 *Astrophys. J. Lett.* **543** L57–60

[56] Blasi P 2002 *Astropart. Phys.* **16** 429–39

[57] Vink J, Yamazaki R, Helder E A and Schure K M 2010 *Astrophys. J.* **722** 1727–34

[58] Haggerty C C and Caprioli D 2020 *Astrophys. J.* **905** 1

[59] Bocchino F, Orlando S, Miceli M and Petruk O 2011 *Astron. Astrophys.* **531** A129

[60] Caprioli D, Haggerty C C and Blasi P 2020 *Astrophys. J.* **905** 2

[61] Shimoda J, Ohira Y, Bamba A, Terada Y, Yamazaki R, Inoue T and Tanaka S J 2022 *Publ. Astron. Soc. Jpn.* **74** 1022–40